APPROVAL SHEET

Title of Thesis: Finite Element Modeling and Modal Testing of a Wind Turbine
Lattice Tower Component

Name of Candidate: Kyle Glazier
                      Master of Science, 2022

Thesis and Abstract Approved: _____

                                 Weidong Zhu, PhD.
                                 Professor
                                 Department of Mechanical Engineering

Date Approved: _____

Curriculum Vitae

Name: Kyle A. Glazier

Degree and date to be conferred: M.S., 2022

Secondary education: Randallstown High School, Randallstown, MD, 2008.

Collegiate institutions attended:
    2017   B.S.   University of Maryland, Baltimore County
    2022   M.S.   University of Maryland, Baltimore County

Major: Mechanical Engineering.

Professional positions held:

Engineer 1   111 West Chesapeake Avenue, Towson, MD

ABSTRACT

Title of Document:	FINITE ELEMENT MODELING AND MODAL TESTING OF WIND TURBINE LATTICE TOWER COMPONENT WITH INTERFERENCE PIN CONNECTIONS.
	Kyle A. Glazier, Master of Science, 2022
Directed By:	Professor Weidong Zhu Department of Mechanical Engineering

Fatigue failures at fastener holes in operating structures are undesirable as it can lead to catastrophic mechanical failures and casualties. Interference pins create interference fits with joined components to reduce stresses around fastener holes and extend the fatigue life of operating structures. In this paper, a novel finite element modeling method is developed for accurate dynamic analysis of a wind turbine lattice tower component with interference pin connections. Installation of interference pins is modeled as a multi-stage process. It causes local changes in stiffness in joined members of the component. The local stiffness changes are accounted for in the finite element model of the component through creation of cylinders to represent interference pins. An experimental setup including a three-dimensional scanning laser vibrometer and a mirror was used to measure out-of-plane and in-plane natural frequencies and mode shapes of the component. Ten out-of-plane modes and one in-

plane mode of the component from its the finite element model are compared with their experimental results to validate its accuracy. The maximum percent difference between theoretical and experimental natural frequencies of the component is 3.27% and modal assurance criterion values between its theoretical and experimental mode shapes are all over 91%.

FINITE ELEMENT MODELING AND MODAL TESTING OF A WIND TURBINE
LATTICE TOWER COMPONENT WITH INTERFERENCE PIN CONNECTIONS

By

Kyle A. Glazier

Thesis submitted to the Faculty of the Graduate School of the
University of Maryland, Baltimore County, in partial fulfillment
of the requirements for the degree of
Master of Science
2022

Acknowledgements

I would like to thank all members of my thesis defense committee Dr. Weidong Zhu, Dr. Ankit Goel, and Dr. Soobum Lee for their time. I would like to thank Dr. Weidong Zhu for his advising and support. I would also like to thank Dr. Yongfeng Xu and Ke Yuan for their help with finite element modeling and modal testing respectively. Finally I would like to thank my family for supporting me through this process.

Table of Contents

List of Tables

List of Figures

Chapter 1: Introduction

Fasteners are needed to form joint connections between parts in many contemporary structures. An interference pin is a type of bolts with interference fits that improves the fatigue life of fastener holes [1,2], since an installed interference pin exerts compressive stresses on fastener holes [3,4]. The neck of an interference pin, as shown in Fig. 1, has a slightly larger outer radius than radii of fastener holes in members to be joined, which introduces interference fits for bolted connections. During installation of an interference pin, material of the pin neck and material of hole surfaces plastically deform around each other, producing wear as shown in Fig. 2. An interference fit is formed from friction between materials of the pin neck and fastener holes. Joined members are further clamped by attaching a nut to the bottom of the interference pin. Interference pin connections are commonly used in aircraft structures and wind turbine lattice towers. Designing structures with interference pin connections requires an understanding of their dynamic behaviors.
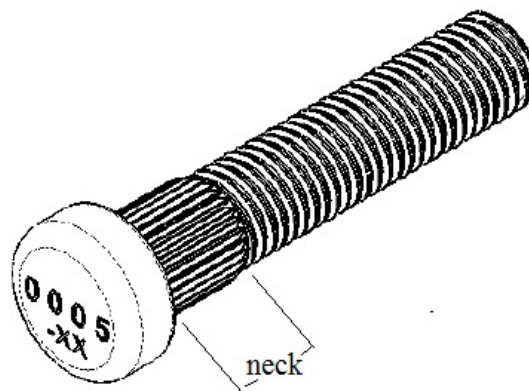
Figure 1 Diagram of an interference pin
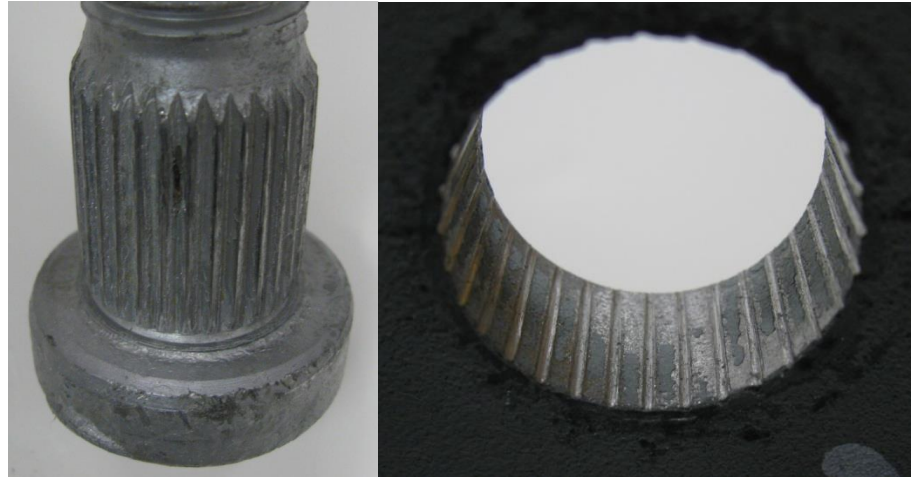
Figure 2 Photos showing wear on the interference pin neck and fastener hole surfaces

Finite element (FE) modeling is a useful tool to simulate and predict dynamic behaviors of structures with interference pin connections. FE modeling has been used to predict the effect of an interference pin connection on the fatigue life of fastener holes [6]. The effect of various interference fits on stresses at fastener hole edges when a remote cyclic stress was applied to a structure was investigated by using FE modeling in Ref. [6]. An FE model was created for an interference pin and a fastener hole in a double shear-lap joint of an aluminum alloy specimen. Installation of the interference pin into fastener holes was first simulated in Ref. [6]; next a cyclic stress was applied to the model of the middle plate of the lap joint. Stress amplitudes at the edge of a fastener hole due to a 10 kN cyclic loading were reduced for higher levels of interference fits. Accuracy of numerical results from the FE model was verified through similar results obtained from experiments. Residual stresses around a fastener hole after installation of an interference pin are commonly believed to be responsible for the improvement of the fatigue life of a structure [7]. It has been shown that installation of interference pins causes stresses to develop around fastener holes [8].

2

An FE simulation of installation of an interference pin into an interference fit joint was successfully created in Ref. [8]. The stress distribution in the vicinity of an interference pin connection in a structure was recorded from its FE model and compared to experimental results for validation purposes. Comparison of FE stresses and experimental stresses showed good agreement. Three-dimensional (3D) FE modeling showed that an interference-fit hybrid bonded bolted (HBB) connection increased load sharing by 10% when compared to a neat-fit HBB connection [9]. In a separate work [10], 3D FE modeling was able to predict the type of failure of a single-lap carbon-fiber reinforced plastic/titanium alloy structure with an interference fit connection. While the work in FE modeling of stresses around an interference pin connection is useful for predicting its failure, a method of predicting dynamic behaviors of an assembled structure is desired.

Difficulties in modeling interference pin connections arise from contacts of numerous surfaces and modeling of stiffnesses at the connections [8]. In an interference pin connection, there are contacts between the interference pin and two clamped members. Accurately modeling every contact within an assembly requires fine meshes that can extend the computation time of a simulation [11]. An FE model that does not include multiple contacts between an interference pin and joined members is desirable. Another difficulty comes from local stiffness changes at an interference pin connection. Installation and clamping of an interference pin produce stiffness changes in its vicinity [11]. Including local stiffness changes is important to accurately model dynamic behaviors of an assembled structure.

Some previous works have been done to create 3D FE models of structures with bolted and riveted joint connections. Research has been done to develop a modeling method where bolted joint connections were replaced with solid cylinders [12]. The parameters of cylinders were meant to emulate local stiffness effects of bolted joint connections. The radius of each cylinder was determined from FE modeling of the contact interface between two joined members. The Young's modulus of each cylinder was calculated by treating the material in the clamped region and the bolt as a set of parallel springs. A 3D FE model of a space frame structure was created with cylinders used in place of bolted joint connections of the structure. When the first 13 modes of the FE model of the space frame structure were compared to experimental results, the maximum percent difference for natural frequencies was 1.72% and modal assurance criterion (MAC) values between theoretical and experimental mode shapes were above 94%. Unlike bolted joint connections, interference pin installation causes wear and deformation of joined members, requiring FE modeling of installation.

A variation of the FE modeling method described in Ref. [12] was applied to modeling of two aluminum strips joined with six riveted joint connections [13]. Plastic deformation of rivets was considered when determining parameters of cylinders. A two-dimensional FE model was created to simulate deformation of rivets following the riveting process. The radius and Young's modulus of each cylinder were calculated using methods similar to those in Ref. [12]. In a 3D FE model of an assembly of two aluminum strips, six riveted joints were replaced with cylinders; 23 out-of-plane modes were identified for the FE model of joined strips, and when

compared to experimental results, the maximum percent difference for natural frequencies was 1.63% and MAC values between theoretical and experimental mode shapes were all over 95%. FE modeling of installation of an interference pin requires a different method from that of a riveted joint connection as they deform differently from each other.

A wind turbine can be mounted on a lattice tower such as that shown in Fig. 3, which requires less material to manufacture than other towers, makes transport easier, and reduces cost. Interference pins can be used in a wind turbine lattice tower to create secure connections between its members. Failure of a wind turbine lattice tower can occur if the rotation speed of its blades coincides with a natural frequency of the tower [14]. The goal of this work is to develop a novel FE modeling method for accurate dynamic analysis of a wind turbine lattice tower component with four interference pin connections, as shown in Fig. 4. The FE software Abaqus is used to create a predictive model for its dynamic behaviors. The wind turbine lattice tower component is made of an L-beam with two flat plates fastened by four interference pin connections (Fig. 4). To solve stated challenges with modeling interference pin connections in structures, a two-stage modeling process is used to create cylinders that can replace interference pin connections. In the first stage of the process, a FE model of installation of an interference pin connection is created. Deformation and contact stresses of joined members from the FE model are used to calculate the radius and Young's modulus of each cylinder. In the second stage of the process, a 3D FE model of the wind turbine lattice tower component is made with cylinders used to connect joined members of the component. Natural frequencies and mode shapes of

the wind turbine lattice tower component are experimentally measured using a 3D scanning laser vibrometer, with a mirror set up to capture response on the side surface of the component. Validity of the FE model of the component is assessed through a percent difference between its theoretical and experimental natural frequencies and MAC values between its theoretical and experimental mode shapes.

This paper is structured as follows. The FE modeling methodology is detailed in Section 2. The rationale behind the two-stage FE modeling process is presented in Section 2.1. FE simulation of installation of an interference pin is discussed in Section 2.2. Model updating of Young's moduli of the L-beam and flat plates are described in Section 2.3, while FE modeling of the wind turbine lattice tower component is described in Section 2.4. The experimental setup used to measure natural frequencies and mode shapes of the wind turbine lattice tower component is detailed in Section 3. Natural frequencies and mode shapes of the FE model of the component and their experimental results are compared in Section 4, and a discussion of results is presented there. Finally, some conclusions of the work are given in Section 5.

Figure 3 Diagram of a wind turbine lattice tower

Figure 4 Photo of a wind turbine lattice tower component with four interference pin

connections

Chapter 2: Finite Element Modeling

This section describes a novel method for accurately modeling the wind turbine lattice tower component with interference pin connections. The Abaqus software is used to create FE models of all members of the component. The primary challenge of modeling the component comes from the difficulty of modeling local stiffness changes that an interference pin connection introduces to the component. Local stiffness changes are due to clamping forces that are difficult to include in a FE model of the component.

2.1 Developing a Predictive Model of the Wind Turbine Lattice Tower Component

Two effects of an interference pin connection on the wind turbine lattice tower component are prevention of displacements of joined members and local stiffness changes. Joined members are not allowed to translate or rotate relative to each other at a connection location due to clamping forces that keep members together. Modeling a connection as a cylinder achieves a similar effect to applying a clamping force while being much easier to model. Dimensions of a cylinder would be the same as those of a contact region of the L-beam and flat plate. Local stiffness changes can be accounted for through a cylinder's Young's modulus. Both the outer radius and stiffness of a contact region are determined through a FE model simulation of installation of an interference pin. The advantage of modeling installation alone is that installation involves numerous interactions between joined members. The L-beam and flat plate have normal and tangential surface interactions. An interference pin and fastener hole have friction interactions as the interference pin neck and fastener hole surface plastically deform around each other. Accurately modeling described interactions requires fine meshes. Such fine meshes are infeasible in a model of the whole wind turbine lattice tower component that contains four interference pin connections, but can be used in a model of an individual interference pin connection. From modeling installation, effects of clamping and local stiffness changes can be fitted to parameters of a cylinder. A cylinder can be much more easily modeled in the wind turbine lattice tower component through meshes on the scale of the rest of the model.

2.2 Simulating Interference Pin Installation

To simulate installation, a 3D FE model of a section of an interference pin, a section of the L-beam, and a section of the flat plate is created. Material properties given in Table 1 are nominal values for each part [15]. Sections are used because they require fewer elements to model, reducing the number of degrees of freedom and therefore lowering the computation time. The interference pin neck contains 30 teeth on its surface. The sections are based on a 12-degree cut of the interference pin and the clamped L-beam and flat plate, as shown in Fig. 5.

Table 1 Material properties of the interference pin and the L-beam and flat plate

	Density (kg/m^3)	Young's modulus (GPa)	Poisson's ratio	Yield stress (MPa)	Fracture strain	Stress at fracture (MPa)
Pin	7850	200	0.3	600	0.14	827
L-beam/flat plate	7850	200	0.3	344	0.16	448
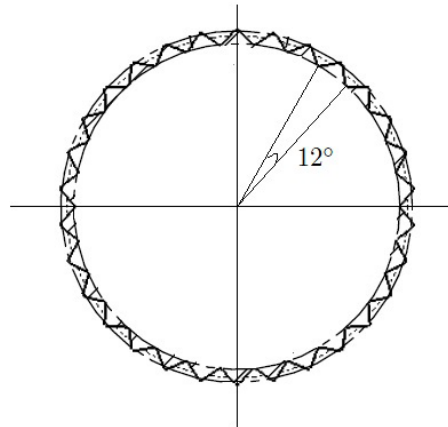
Figure 5 Diagram of an interference pin cross-section

Interference pin, L-beam, and flat plate sections are positioned so that their origins coincide, as shown in Fig. 6. The bottom surface of the interference pin section is positioned just above the top surface of the L-beam section. To represent effects of surrounding materials on interference pin, L-beam, and flat plate sections, boundary conditions depicted in Fig. 7 are placed on cut surfaces to restrict normal displacements. The friction coefficient of 0.2 is used for contacts among interference pin, L-beam, and flat plate sections. Plastic behaviors are enabled for interference pin, L-beam, and flat plate sections so that plastic deformation of the installation process can be modeled. Interference pin, L-beam, and flat plate sections are meshed so that meshes near contact surfaces are finer than those further away.
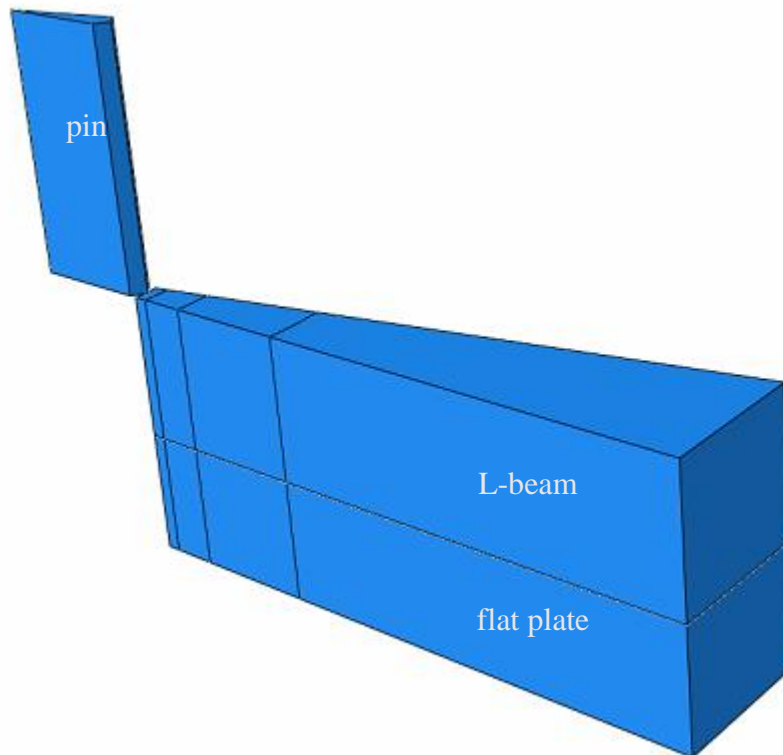
Figure 6 FE model of the interference pin, L-beam, and flat plate section assembly
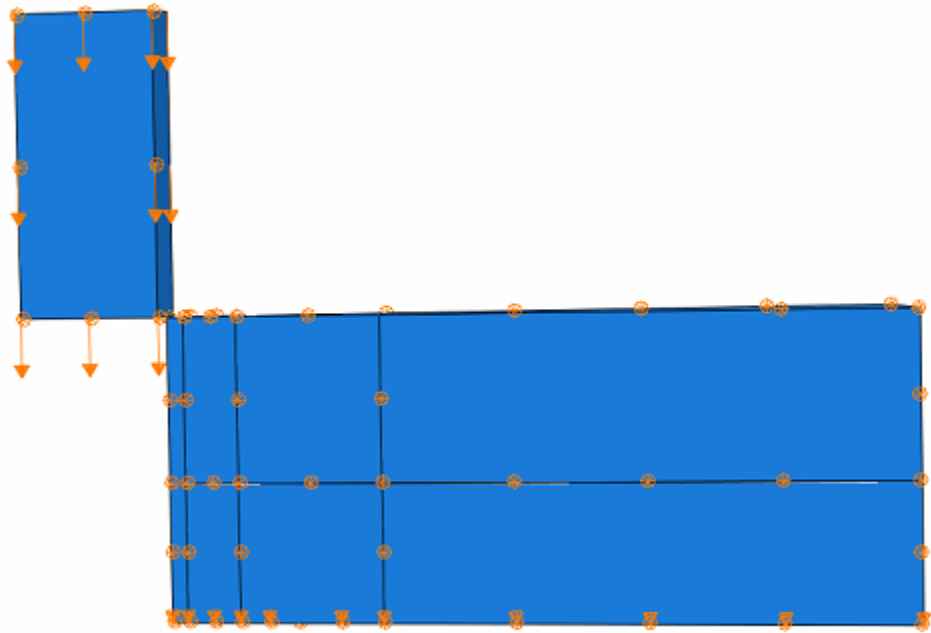
Figure 7 Boundary conditions on interference pin, L-beam, and flat plate sections during installation

FE model simulation of installation consists of two steps. In the first step, the interference pin section is driven into L-beam and flat plate sections by displacing elements of the interference pin section downward a distance equal to the combined thickness of L-beam and flat plate sections. In the second step, a clamping stress of 150 MPa is applied to L-beam and flat plate sections, as shown in Fig. 8. The clamping stress acts over an area equal to the area of the interference pin head that is in contact with the L-beam. The clamping stress is applied for 9.6 seconds to allow time for stresses and deformation to converge.
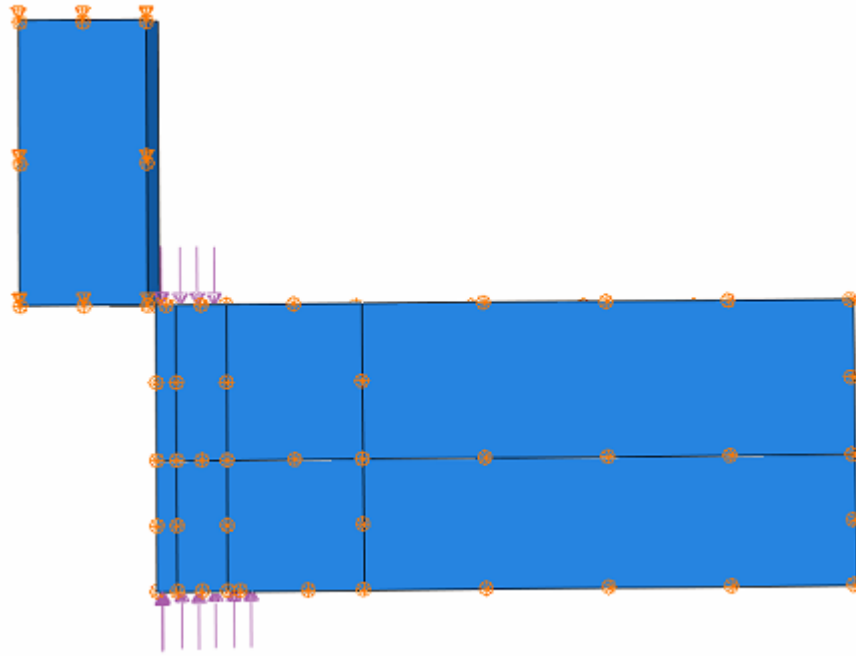
Figure 8 Boundary conditions on interference pin, L-beam, and flat plate sections and applied stress in the clamping step

At completion of the clamping step, the area and stiffness of the contact region can be determined. In the contact region, L-beam and flat plate sections are in contact due to the applied clamping stress. Stresses arise on contact surfaces of L-beam and flat plate sections, as shown in Fig. 9. The area of the contact region is therefore the area of L-beam and flat plate section surfaces with non-zero contact stresses. Because clamping is a semi-static process, the area of the contact region fluctuates with time before converging to a constant value, as shown in Fig. 10. The outer radius of the area of the contact region is obtained from convergence of peaks and troughs of FE model data over the 9.6 second duration in Fig. 10. From convergence of data, it is seen that the outer radius of the area of the contact region is

0.0278 m. The radius of the cylinder is made 0.0278 m to match the result of the FE

model simulation.

(a)
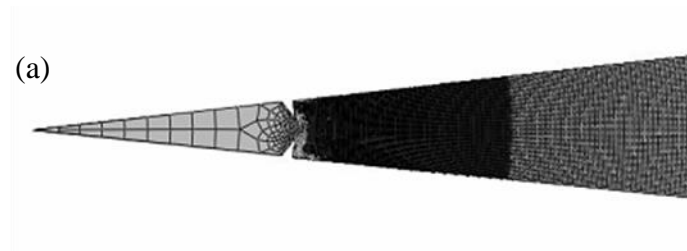
Area of contact region at t = 8.5 s

(b)
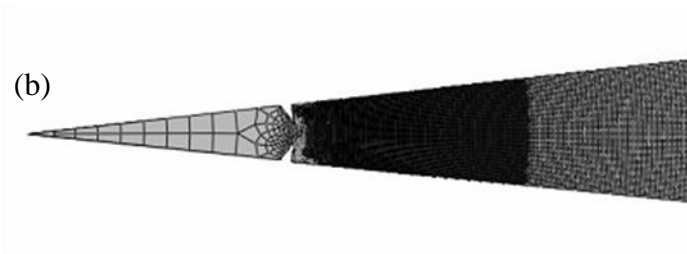
Area of contact region at t = 9.0 s

(c)
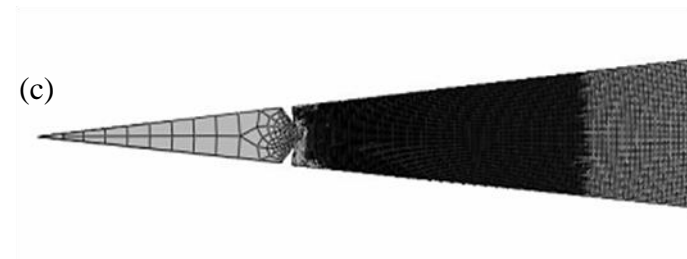
Area of contact region at t = 9.5 s

Figure 9 Contact regions indicated by dark-shaded regions at different times t: (a) 8.5

s, (b) 9.0 s, and (c) 9.5 s; non-contact regions are shown as light-shaded regions
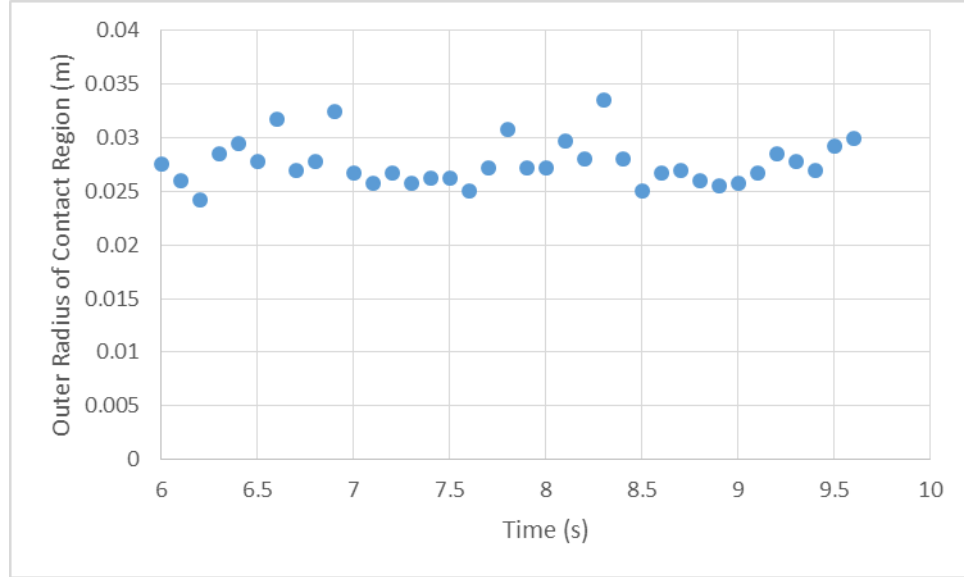
Figure 10 Variation of the outer radius of the contact region with time

The only remaining unknown parameter of the cylinder is its Young's modulus that can be obtained from stress-strain behaviors of L-beam and flat plate sections in the contact region. The displacement in the Z direction is averaged over several nodes within the contact region on L-beam and flat plate section surfaces after the clamping stress is applied. Directions of displacements of nodes on L-beam and flat plate sections are parallel to the direction of the applied clamping stress. Similar to how the radius of the contact region is found, the average displacement of nodes is the converged value over the 10 second duration in the second step, as shown in Fig. 11. The difference in average displacement between the top of the L-beam section and the bottom of the flat plate section is found to be 1.28×10^{-5} m. The Young's modulus of L-beam and flat plate sections within the contact region can be calculated from the stress-strain relation for a material within the elastic region:

$$E_p = \frac{FL}{A\Delta L} \tag{1}$$

15

where E_p is the Young's modulus of L-beam and flat plate sections within the contact region, F is the clamping force, A is the area of the contact region, L is the combined thickness of L-beam and flat plate sections, and ΔL is the difference in displacement between L-beam and flat plate sections previously determined. When values of the four variables are placed into Eq. (1), the Young's modulus of L-beam and flat plate sections is calculated to be 135 GPa. The calculated Young's modulus shows that Young's moduli of L-beam and flat plate sections within the contact region are lowered due to clamping. While Young's moduli of L-beam and flat plate sections within the contact region are changed, the Young's modulus of the interference pin remains unchanged as it does not undergo clamping. The Young's modulus of the cylinder is calculated through a weighted average of Young's moduli of interference pin, L-beam, and flat plate sections:

$$E_c = \frac{E_p A_p + E_i A_i}{A_p + A_i} \qquad (2)$$

where A_p and A_i are the area of the contact region and the cross-sectional area of the interference pin, respectively, and E_i is the Young's modulus of the interference pin. The area of the contact region is the difference between the area within the outer radius of the contact region and the area of the fastener hole:

$$A_p = \frac{\pi}{30} \times (0.0278^2 - 0.0135^2) \ m^2 = 6.18 \times 10^{-5} \ m^2 \qquad (3)$$

The cross-sectional area of the interference pin is

$$A_i = \frac{\pi}{30} \times (0.0135 \ m)^2 = 1.91 \times 10^{-5} \ m^2 \qquad (4)$$

16

The Young's modulus of the cylinder is calculated to be 150 GPa. With two unknown parameters of the cylinder determined, the cylinder can be used to model interference pin connections in a FE model of the wind turbine lattice tower component.
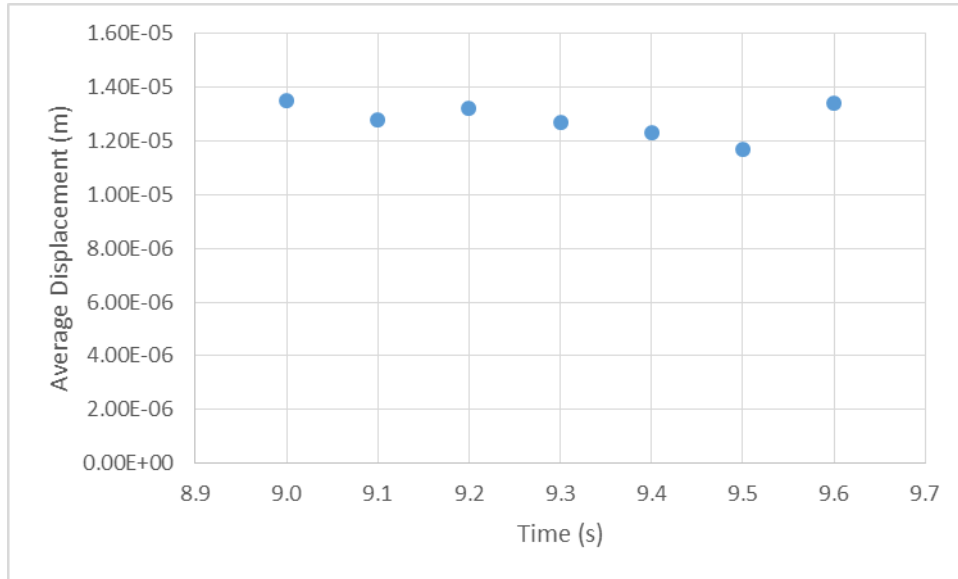

Figure 11 Variation of the average displacement of L-beam and flat plate sections with time

2.3 Updating Young's Moduli of the L-beam and Flat Plate in FE Model

It is important to control factors that can influence dynamic behaviors of a FE model of the wind turbine lattice tower component, such as FE modeling of the L-beam and flat plates. An error with a given Young's modulus for either the L-beam or flat plates in the FE model can result in less accuracy when natural frequencies and mode shapes of the FE model of the component are compared to its experimental results. Model updating is used to yield accurate approximations of Young's moduli of the L-beam and flat plates. Young's moduli are updated because they are material properties that can have uncertainties.

Modal testing is performed on the L-beam and a flat plate shown in Fig. 12 to obtain their experimental natural frequencies. Reflective tapes are attached to surfaces of the L-beam and flat plate to maximize back-scattering of laser light. Strings are used to hang the L-beam and flat plate to simulate their free boundary conditions. The hung L-beam and flat plate are each excited by a MB Dynamics MODAL-50 shaker with a periodic chirp signal with a frequency range of 0-5000 Hz. A commercial 3D scanning laser Doppler vibrometer (SLDV) Polytec PSV-500-3D is used to capture 3D responses of the L-beam and flat plate. Frequency spectra and identified natural frequencies of elastic modes of the L-beam and flat plate are shown in Fig. 13a and 13b, respectively, where frequency spectra are plotted as black solid lines and identified natural frequencies of elastic modes are marked by red circles. Seven experimental natural frequencies of elastic modes of the L-beam and eight experimental natural frequencies of elastic modes of the flat plate are identified in the frequency range.
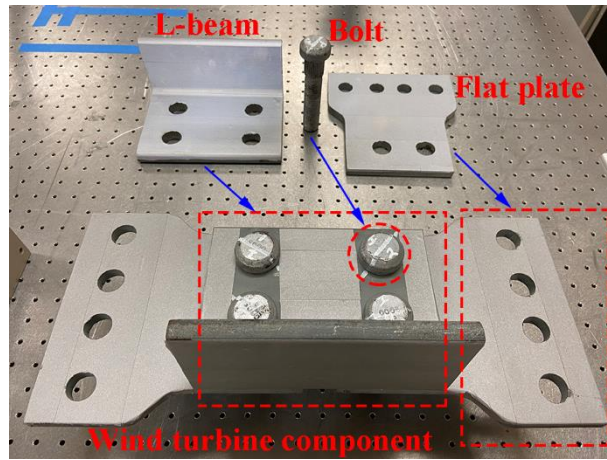
Figure 12 Main members of the wind turbine lattice tower component
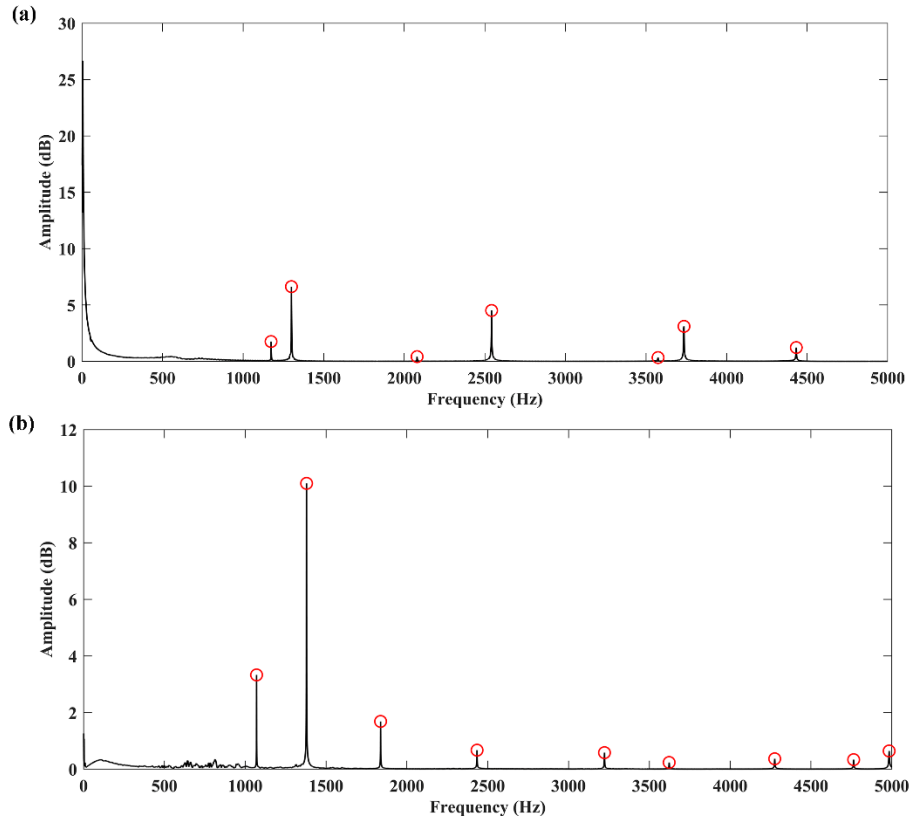
Figure 13 Frequency spectra of the (a) L-beam and (b) flat plate that are plotted as

black solid lines with identified natural frequencies of elastic modes marked by red

circles

FE models are created for the L-beam and flat plates, as shown in Fig. 14.

Dimensions of models are based on measurements of experimental specimens.

Features such as holes in flat plates and the fillet of the L-beam can affect their

natural frequencies and mode shapes so care is taken to ensure their sizes and

locations match their test specimens'. The L-beam is meshed using C3D4

tetrahedrons due to its fillet, while flat plates are meshed using C3D8R hexahedrons.

Sizes of elements are determined by convergence of models. The mesh density is

sufficient to account for inaccuracies introduced by using C3D4 tetrahedrons. Both

models are given free boundary conditions to match boundaries of test specimens.
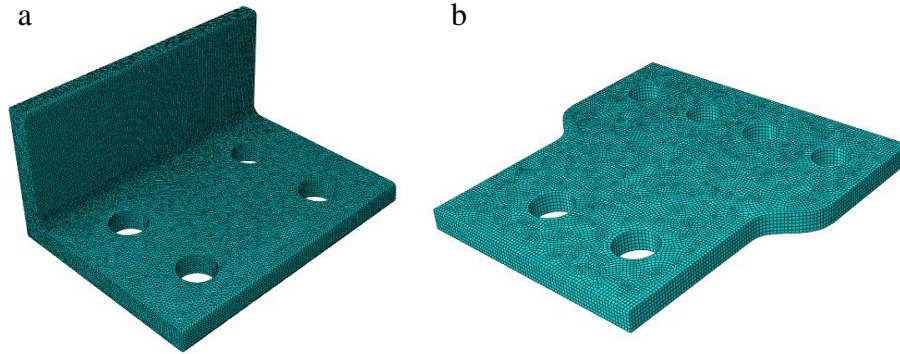
Figure 14 FE Models of (a) the L-beam and (b) a flat plate

Young's moduli of the L-beam and flat plates are initially set to a nominal

value of 200 GPa. Young's moduli are updated by minimizing the maximum percent

difference between theoretical and experimental natural frequencies. Young's moduli

are changed to minimize the maximum percent difference between theoretical and

experimental natural frequencies After model updating, the L-beam and flat plates

have Young's moduli of 205 GPa and 206 GPa, respectively. The maximum percent

difference between theoretical and experimental natural frequencies of the L-beam is

0.69% while that of the flat plate is 1.09%, as shown in Table 2 and Table 3,

respectively. Normal values of the density and Poisson's ratio of the L-beam and flat

plates are used. With updated Young's moduli of the L-beam and flat plates, their FE

models are considered accurate. With the L-beam and flat plate models updated, the

only factor that can significantly influence dynamic behaviors of the FE model of the

wind turbine lattice tower component would be modeling of interference pin

connections.

Table 2 Comparison between natural frequencies of the L-beam from its updated FE

model and those from its modal test

Mode No.	FE model (Hz)	Modal test (Hz)	Difference (%)
1	1167	1173	0.48
2	1293	1300	0.52
3	2075	2080	0.24
4	2539	2542	0.13
5	3573	3575	0.05
6	3762	3736	-0.69
7	4441	4433	-0.17

Table 3 Comparison between natural frequencies of the flat plate from its updated FE

model and those from its modal test

Mode No.	FE model (Hz)	Modal test (Hz)	Difference (%)
1	1072	1070	-0.20
2	1380	1380	0
3	1823	1838	0.81
4	2420	2434	0.60
5	3230	3223	-0.23
6	3657	3623	-0.95
7	4246	4276	0.70
8	4712	4764	1.09

2.4 Developing the FE Model of the Wind Turbine Lattice Tower Component

FE models of the L-beam and flat plates from Section 2.3 are included in the FE model of the wind turbine lattice tower component, along with that of a cylinder with previously determined dimensions and material properties, as shown in Fig. 15. An alteration is made to L-beam and flat plate models by making the radius of fastener holes the same as that of the cylinder, ensuring that there is no overlap between the cylinder and the L-beam and flat plates when they are tied to each other. The assembled FE model of the wind turbine lattice tower component is shown in Fig. 16, where models of the interference pin heads, interference pin bolts, nuts, and washers are also created. Dynamic behaviors of external parts of interference pin bolts are not examined in this work and their inclusion in the model is for the sake of accuracy. The L-beam and flat plates are assembled to the same positions as those in their experimental counterparts. Each of four cylinders is placed so that its center axis coincides with the center axis of one of fastener holes in the L-beam and flat plates. Tie constraints are used to attach four cylinders to the L-beam and flat plates. It is important to enable contacts between surfaces of the L-beam and flat plates. Surfaces of the L-beam and flat plates are outside the determined contact region and so they are given frictionless contacts. The wind turbine lattice tower component model is given free boundary conditions. The entire wind turbine lattice tower component model is meshed using an element size of 0.002 m as that is where results begin to converge. Ten out-of-plane elastic modes and one in-plane elastic mode of the component are found within the 2000 Hz frequency range. Reducing the element size to 0.0015 m produces a percent difference less than 1% when natural frequencies are

compared with an element size of 0.002 m, which shows convergence is reached. Accuracy of the created theoretical model is validated through a comparison with experimental results.
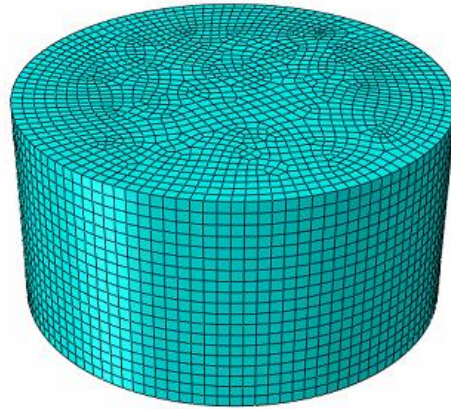

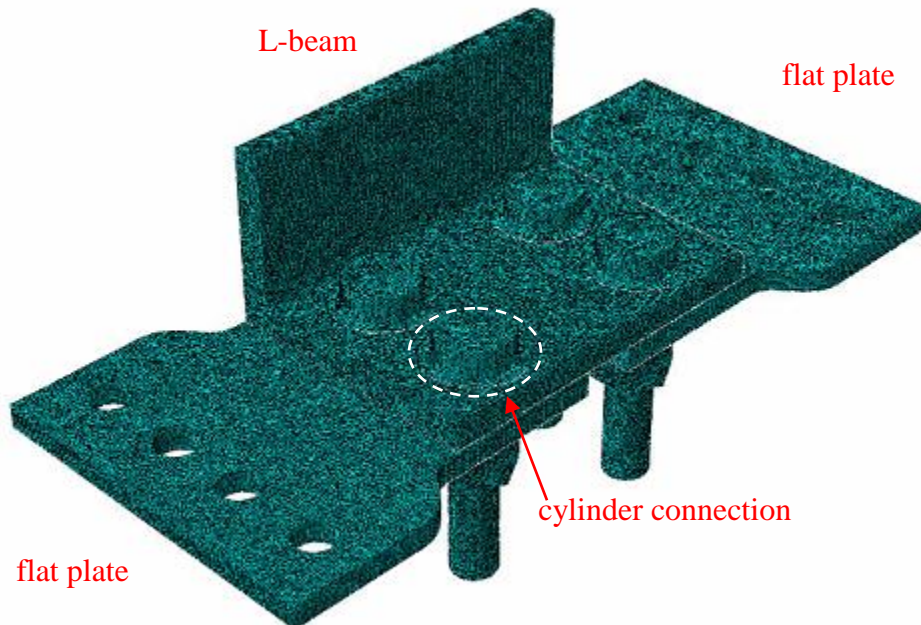Figure 15 FE model of the cylinder

Figure 16 FE model of the wind turbine lattice tower component

Chapter 3: Modal Test of the Wind Turbine Lattice Tower Component

A shaker test of the wind turbine lattice tower component is conducted to obtain its experimental natural frequencies and mode shapes. The wind turbine lattice tower component is hung by a string, as shown in Fig. 17, to simulate its free boundary conditions. The surface of the wind turbine lattice tower component that is almost normal to the laser beam of the middle laser head of the SLDV is referred to as the front surface of the component, while the surface almost parallel to it is referred to as the side surface, as shown in Fig. 18, where the mirror is used to reflect laser beams from three laser heads to measure response of the side surface of the component. Excitation and measurement devices are the same as those described in Section 2.3 with an additional mirror used here. Calibration of the SLDV is conducted, and grids of measurement points on front and side surfaces of the component are designed, as shown in Fig. 18, where there are 156 measurement points are on the front surface and 81 points on the side surface. 3D coordinates of measurement points on front and side surfaces of the component are captured. Note that a global coordinate system based on the front surface of the component is created in the experiment, as shown in Fig. 18(b), whose X axis is along its in-plane horizontal direction, Y axis is along its in-plane vertical direction, and Z axis is along its out-of-plane direction. Eleven elastic modes are found within the 2000 Hz frequency range, as shown in Fig. 19, where the spectrum of response along the X direction is plotted as a black solid line and that along the Z direction is plotted as a blue dashed line with identified natural frequencies marked by red circles. The highest natural frequency of rigid-body modes of the wind turbine lattice tower component is 1.25 Hz, which is much less than 10%

of the natural frequency (429 Hz) of its first elastic mode; this validates its free boundary conditions. Excitations of the wind turbine lattice tower component are in the Z direction for the ten out-of-plane modes and in the X direction for the one in-plane mode.
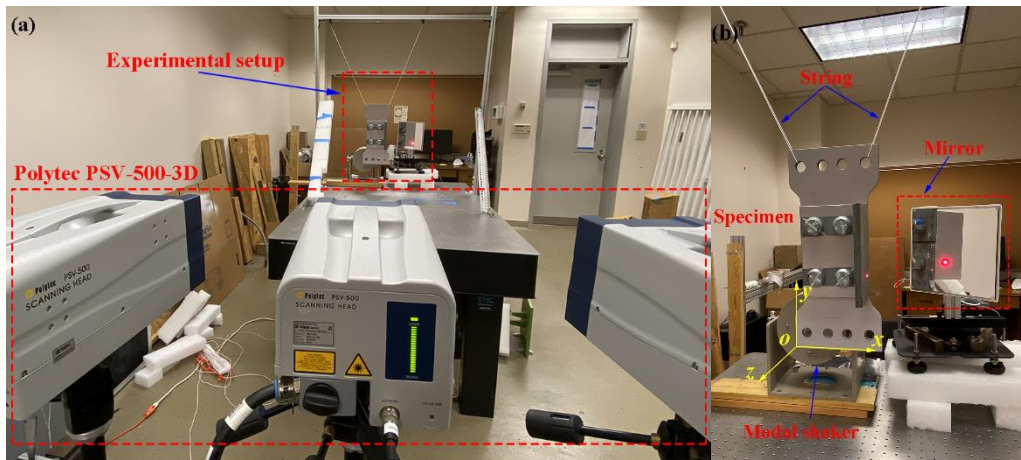
Figure 17 (a) Experimental setup and measurement device Polytec PSV-500-3D, and (b) an expanded view of the experimental setup
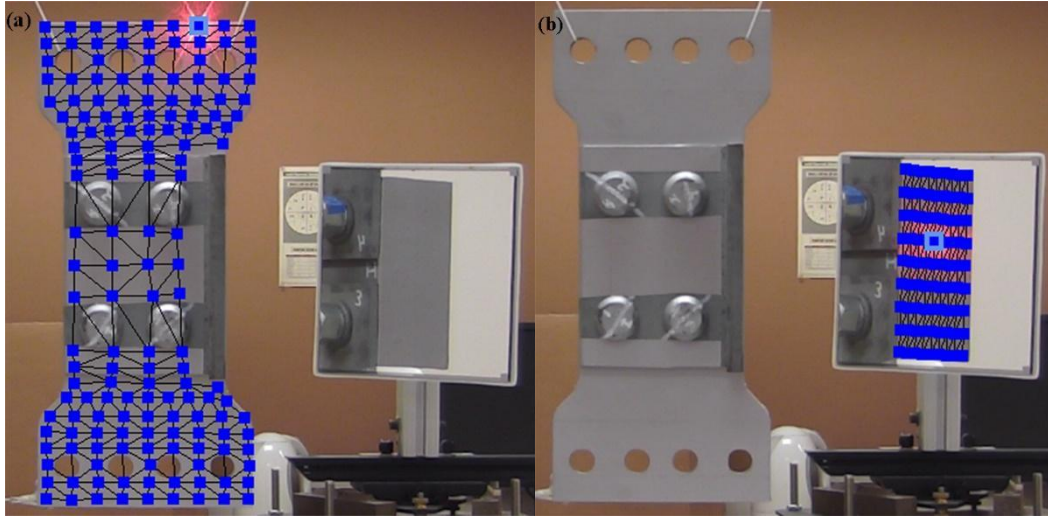
Figure 18 Grids of measurement points on (a) front and (b) side surfaces of the wind

turbine lattice tower component
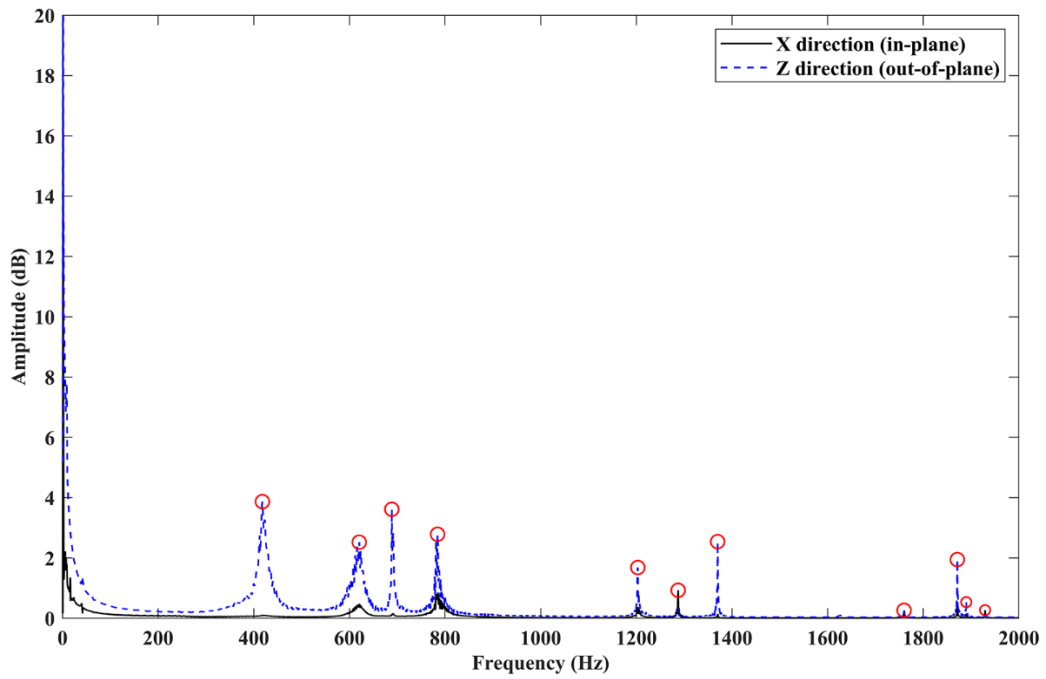
Figure 19 Frequency spectrum of the wind turbine lattice tower component, where the

spectrum of the response along the X direction is plotted as a black solid line and that

along the z direction is plotted as a blue dashed line with identified natural

frequencies of elastic modes marked by red circles

Chapter 4: Results and Discussion

Natural frequencies of the first 11 elastic modes are theoretically and experimentally identified within the 2000 Hz frequency range for the wind turbine lattice tower component, as shown in Table 4, and a percent difference is calculated there between theoretical and experimental natural frequencies of each mode. The maximum percent difference is 3.27%, showing good agreement between results from the FE model and the modal test.

Table 4 Percent difference between theoretical and experimental natural frequencies of the wind turbine lattice tower component

| Mode No.	Theory (Hz)	Experiment (Hz)	Difference (%)
1	422	429	-1.63
2	629	622	1.13
3	678	691	-1.88
4	805	796	1.13
5	1221	1203	1.5
6	1328	1286	3.27
7	1388	1369	1.39
8	1815	1759	3.18
9	1876	1870	0.32
10	1903	1890	0.69
11	1983	1932	2.64

Theoretical and experimental mode shapes of the wind turbine lattice tower component are compared to provide a second measure of the validity of the FE model. A MAC value is used to quantify the degree of correlation between theoretical and experimental mode shapes, which is calculated by

$$\text{MAC} = \frac{[\sum_{j=1}^{n}\{U_{ej}\}^{H}\{U_{tj}\}]^{2}}{(\sum_{j=1}^{n}(\{U_{ej}\}^{H}\{U_{ej}\}))(\sum_{j=1}^{n}(\{U_{tj}\}^{H}\{U_{tj}\}))} \qquad (5)$$

where H denotes the Hermitian transpose, n is the number of measurement points, and U_{ej} and U_{tj} are components of displacement vectors at the measurement point j for theoretical and experimental mode shapes, respectively [16]. MAC values range from 0 to 1 with a value close to 0 indicating low correlation and a value close to 1 indicating high correlation.

One can determine whether each theoretical elastic mode shape in Fig. 20(a) mainly consists of in-plane or out-of-plane vibrations. It is important to identify the type of mode shapes so that appropriate displacement directions can be used in MAC value calculations. Including displacements in directions that are perpendicular to the excitation direction reduces correlation between theoretical and experimental mode shapes. Modes 1 through 10 are out-of-plane modes and as such only front-surface out-of-plane displacements are used in MAC value calculations. Mode 11 is the only in-plane mode, as depicted in Fig. 20, and it is the only mode where front-surface in-plane displacements are used. All modes of the side surface are out-of-plane modes, and all points on the side surface have their out-of-plane displacements used in MAC value calculations.

(a)

Mode 1

Mode 2

Mode 3

Mode 4

Mode 5

Mode 6

Mode 7

Mode 8

Mode 9

Mode 10

Mode 11

(b)
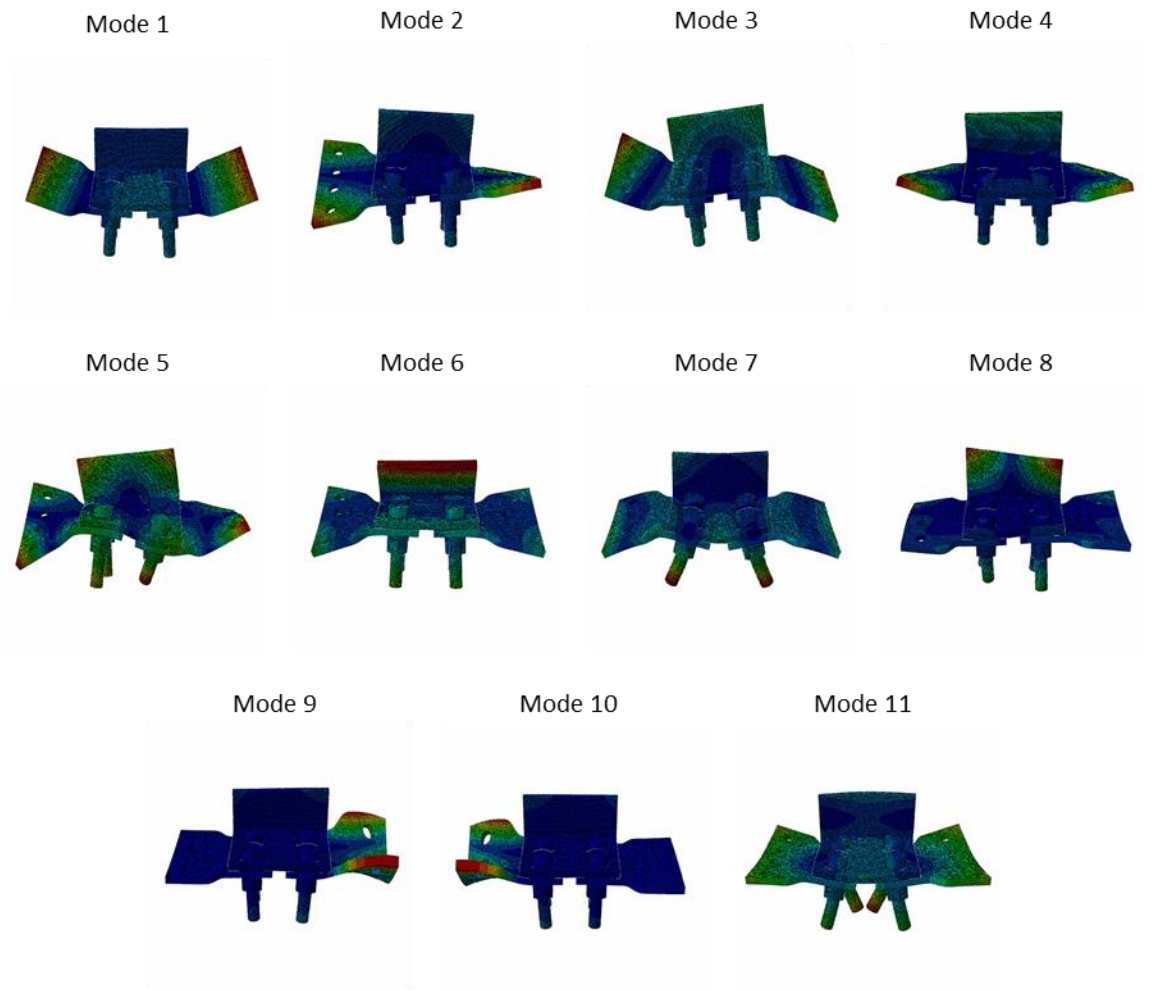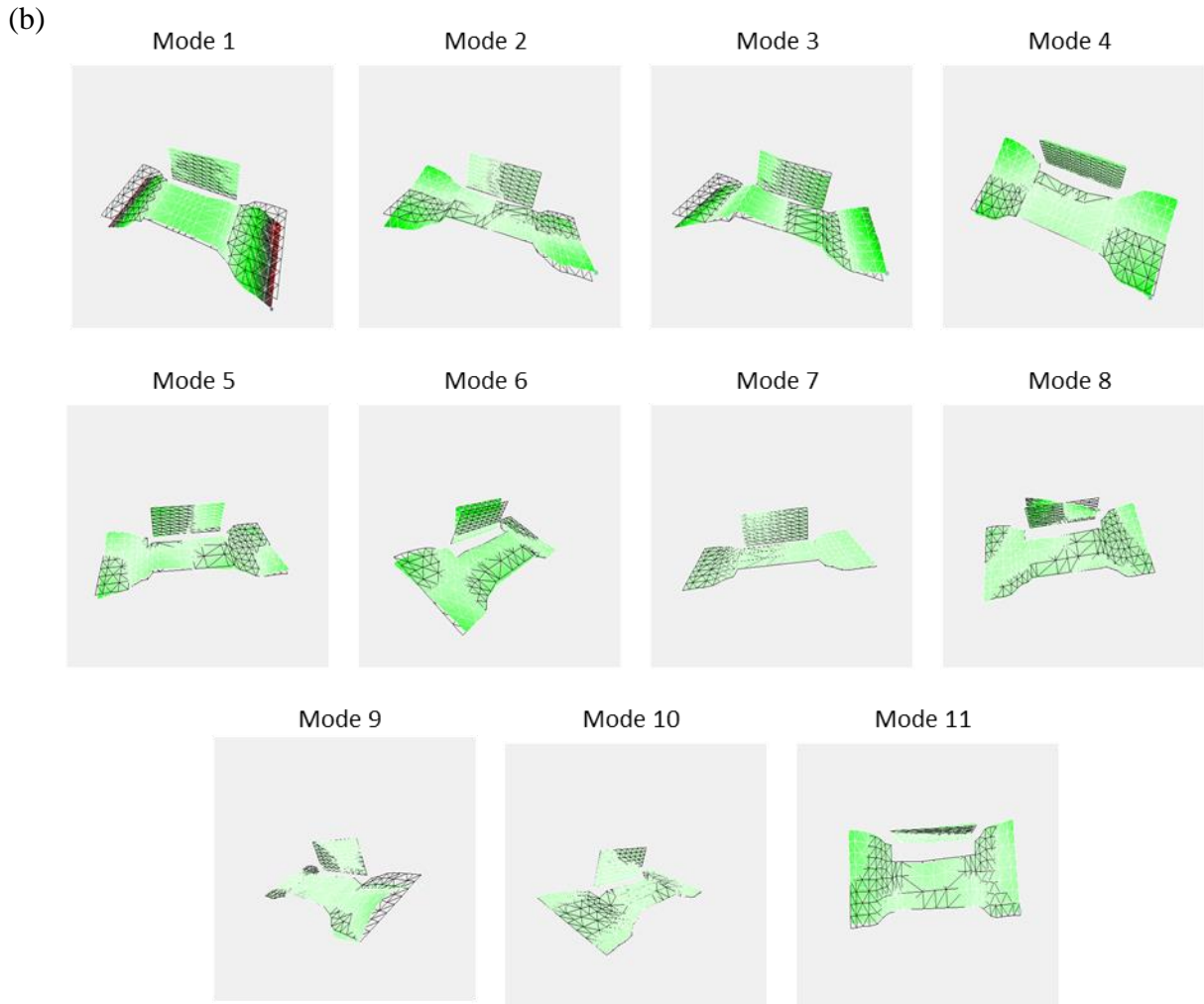
Figure 20 Eleven (a) theoretical and (b) experimental elastic mode shapes of the wind turbine lattice tower component

A MAC value is calculated for every combination of theoretical and experimental mode shapes and placed in Table 5. All 237 measurement points taken during the shaker test are used to perform MAC value calculations. Diagonal MAC values in Table 5 are all above 91% while off-diagonal values are all less than 30%, showing a high amount of similarity between theoretical and experimental mode shapes.

Table 5 MAC values for the first 11 elastic mode shapes of the wind turbine lattice tower component, where FE1 and EXP1 indicate the first theoretical and experimental mode shapes, respectively, and similar notations are used for other modes

	EXP1	EXP2	EXP3	EXP4	EXP5	EXP6	EXP7	EXP8	EXP9	EXP10	EXP11
FE1	0.98	0	0.01	0.01	0	0.01	0.16	0	0	0.01	0.01
FE2	0	0.98	0.02	0	0.30	0	0	0.02	0.04	0	0.01
FE3	0	0.05	0.99	0	0	0	0.01	0.01	0	0	0.03
FE4	0	0	0	0.99	0.01	0	0.03	0	0.02	0	0.1
FE5	0	0.26	0	0.01	0.97	0	0.01	0.17	0.03	0.02	0.02
FE6	0	0	0	0.01	0	0.97	0.02	0	0	0	0
FE7	0.12	0.01	0.02	0.03	0.03	0.06	0.92	0	0.08	0.01	0.05
FE8	0	0.02	0	0	0.15	0	0	0.95	0	0.01	0.02
FE9	0	0	0	0	0	0	0.03	0.01	0.96	0.04	0.04
FE10	0	0	0	0	0.01	0	0.02	0	0.09	0.93	0.04
FE11	0.29	0	0.01	0.08	0	0	0.11	0	0.03	0	0.98

Modes 2 and 5 shown in Table 5 have relatively high off-diagonal MAC values at 26% and 30%. Flat plate members of the wind turbine lattice tower component undergo similar torsion modes in both modes 2 and 5. Note that 128 measurement points are used to measure responses of flat plate members, while only 28 measurement points are used to measure response of the front surface of the L-beam member. More measurement points on the front surface of the L-beam member can better distinguish these two mode shapes and reduce their MAC values.

The (11, 1) entry of the MAC matrix in Table 5 has a value of 29%, which is significantly greater than the (1, 11) entry of the MAC matrix, that has a value of 1%. The wind turbine lattice tower component is excited in the out-of-plane direction to obtain its experimental mode shapes for modes 1 through 10, resulting in low signal-to-noise ratios in its in-plane response measurement. The effect of a low signal-to-noise ratio in-plane response measurement is most pronounced in estimating the first experimental mode shape because the ratio of the in-plane displacement to the maximum out-of-plane displacement for the first mode is much lower than those for modes 2 through 10. The 11th experimental mode shape of the wind turbine lattice tower component is excited with in-plane excitation, and as a result, the signal-to-noise ratio is high in its in-plane response measurement.

Different clamping stresses are applied during the interference pin installation simulation to justify the choice of the clamping stress. Clamping stresses below 50 MPa resulted in incomplete contact between the L-beam and flat plate sections. Above 50 MPa the outer radius of the contact region was not sensitive to the clamping stress applied. The 150 MPa stress simulates a tight clamping situation.

Chapter 5: Conclusion

A novel FE modeling method is developed for accurate dynamic analysis of a wind turbine lattice tower component with interference pin connections. A two-step process simulates installation of an interference pin in the component to obtain parameters of a cylinder that can represent dynamic behaviors of the interference pin connection. A shaker test involving a 3D SLDV and a mirror is used to obtain out-of-plane and in-plane frequency spectra and mode shapes of the wind tower lattice tower component. The created FE model can predict the first 11 natural frequencies and mode shapes of the wind turbine lattice tower component with a good degree of accuracy when compared to results from the shaker test. The methodology developed in this work for modeling interference pin connections with cylinders is shown to be effective.

Bibliography

[1] Crews, J. H. 1975, "Analytical and Experimental Investigation of Fatigue in a Sheet Specimen with an Interference-Fit Bolt." *National Aeronautics and Space Administration*, https://ntrs.nasa.gov/api/citations/19750019346/downloads/19750019346.pdf

[2] Wei, J., Jiao, G., Jia, P., and Huang, T., 2013, "The Effect of Interference Fit Size on the Fatigue Life of Bolted Joints in Composite Laminates." *Composites Part B: Engineering*, 53, 62–68. https://doi.org/10.1016/j.compositesb.2013.04.048.

[3] Wu, T., Zhang, K., Cheng, H., Liu, P., Song, D., and Li, Y., 2016 "Analytical Modeling for Stress Distribution around Interference Fit Holes on Pinned Composite Plates under Tensile Load." *Composites Part B: Engineering*, 100, 176–185. https://doi.org/10.1016/j.compositesb.2016.06.011.

[4] Jiang, J., Bi, Y., Dong, H., Ke, Y., Fan, X., and Du, K., 2014 "Influence of Interference Fit Size on Hole Deformation and Residual Stress in Hi-Lock Bolt Insertion." *Proceedings of the Institution of Mechanical Engineers, Part C: Journal of Mechanical Engineering Science*, 228(18), 3296–3305. https://doi.org/10.1177/0954406214531250.

[5] Ibrahim, R.A., and Pettit, C.L., 2005 "Uncertainties and Dynamic Problems of Bolted Joints and Other Fasteners." *Journal of Sound and Vibration*, 279(3-5), 857–936. https://doi.org/10.1016/j.jsv.2003.11.064.

[6] Chakherlou, T.N., Mirzajanzadeh, M., and Vogwell, J., 2009 "Experimental and Numerical Investigations into the Effect of an Interference Fit on the Fatigue Life of Double Shear Lap Joints." *Engineering Failure Analysis*, 16(7), 2066–2080. https://doi.org/10.1016/j.engfailanal.2009.01.009.

[7] Sun, Y., Hu, W., Shen, F., Meng, Q., Xu, Y., 2016 "Numerical Simulations of the Fatigue Damage Evolution at a Fastener Hole Treated by Cold Expansion or with Interference Fit Pin." *International Journal of Mechanical Sciences*, 107, 188–200. https://doi.org/10.1016/j.ijmecsci.2016.01.015.

[8] Song, D., Li, Y., Zhang, K., Liu, P., Cheng, H., and Wu, T., 2015 "Stress Distribution Modeling for Interference-Fit Area of Each Individual Layer around Composite Laminates Joint." *Composites Part B: Engineering*, 78, 469–479. https://doi.org/10.1016/j.compositesb.2015.04.013.

[9] Raju, K.P., Bodjona, K., Lim, G. , and Lessard, L., 2016 "Improving Load Sharing in Hybrid Bonded/Bolted Composite Joints Using an Interference-Fit Bolt." *Composite Structures*, 149, 329–338. https://doi.org/10.1016/j.compstruct.2016.04.025.

[10] Li, J., Li, Y., Zhang, K., Liu, P., and Zou, P., 2015 "Interface Damage Behaviour during Interference-Fit Bolt Installation Process for CFRP/Ti Alloy Joining Structure." *Fatigue & Fracture of Engineering Materials & Structures*, 38(11), 1359–1371. https://doi.org/10.1111/ffe.12313.

[11] Kim, S, He, B., Shim, C., and Kim, D., 2013 "An Experimental and Numerical Study on the Interference-Fit Pin Installation Process for Cross-Ply Glass Fiber Reinforced Plastics (GFRP)." *Composites Part B: Engineering*, 54, 153–162. https://doi.org/10.1016/j.compositesb.2013.05.006.

[12] He, K., and Zhu, W. D., 2011 "Finite Element Modeling of Structures With L-Shaped Beams and Bolted Joints." *ASME Journal of Vibration and Acoustics*, 133(1), 011011. https://doi-org.proxy-bc.researchport.umd.edu/10.1115/1.4001840.

[13] Kim, J. S., Xu, Y.F., and Zhu, W.D., 2020 "Linear Finite Element Modeling of Joined Structures with Riveted Connections." *Journal of Vibration and Acoustics*, 142(2). https://doi.org/10.1115/1.4045582.

[14] Nezamolmolki, D., and Shooshtari, A., 2016 "Investigation of Nonlinear Dynamic Behavior of Lattice Structure Wind Turbines." *Renewable Energy*, 97, 33–46. https://doi.org/10.1016/j.renene.2016.05.070.

[15] "GE Launches Advanced Technology Space Frame Tower for Wind Turbines." 10 Mar. 2014, https://www.ge.com/news/press-releases/ge-launches-advanced-technology-space-frame-tower-wind-turbines. Accessed 30 Apr. 2023.

[16] Ewins, D.J. 2000 *Modal Testing: Theory, Practice and Application*. 2nd ed., Research Studies Press. 424–427.